

See discussions, stats, and author profiles for this publication at: <https://www.researchgate.net/publication/6720918>

Binary Tree-Based Generic Demosaicing Algorithm for Multispectral Filter Arrays

Article in *IEEE Transactions on Image Processing* · December 2006

DOI: 10.1109/TIP.2006.877476 · Source: PubMed

CITATIONS

111

READS

746

4 authors, including:



Lidan Miao

Microsoft

21 PUBLICATIONS 1,205 CITATIONS

[SEE PROFILE](#)



Hairong Qi

University of Tennessee

307 PUBLICATIONS 10,021 CITATIONS

[SEE PROFILE](#)



Wesley Snyder

North Carolina State University

199 PUBLICATIONS 3,769 CITATIONS

[SEE PROFILE](#)

Binary Tree-based Generic Demosaicking Algorithm for Multispectral Filter Arrays

Lidan Miao, *Student Member, IEEE*, Hairong Qi, *Senior Member, IEEE*, Rajeev Ramanath, *Member, IEEE*, and Wesley E. Snyder, *Senior Member, IEEE*

Abstract—In this paper, we extend the idea of using mosaicked color filter array (CFA) in color imaging, which has been widely adopted in the digital color camera industry, to the use of multispectral filter array (MSFA) in multispectral imaging. The filter array technique can help reduce the cost, achieve exact registration, and improve the robustness of the imaging system. However, the extension from CFA to MSFA is not straightforward. First, most CFAs only deal with a few bands (3 or 4) within the narrow visual spectral region, while the design of MSFA needs to handle the arrangement of multiple bands (more than 3) across a much wider spectral range. Second, most existing CFA demosaicking algorithms assume the fixed Bayer CFA and are confined to properties only existed in the color domain. Therefore, they cannot be directly applied to multispectral demosaicking. The main challenges faced in multispectral demosaicking is how to design a generic algorithm that can handle the more diversified MSFA patterns, and how to improve performance with a coarser spatial resolution and a less degree of spectral correlation. In this paper, we present a binary tree based generic demosaicking method. Two metrics are used to evaluate the generic algorithm, including the root mean-square error (RMSE) for reconstruction performance and the classification accuracy for target discrimination performance. Experimental results show that the demosaicked images present low RMSE (less than 7) and comparable classification performance as original images. These results support that MSFA technique can be applied to multispectral imaging with unique advantages.

Index Terms—Binary tree, color filter array (CFA), demosaicking, edge-sensing interpolation, mosaicking, multispectral filter array (MSFA), spectral correlation.

I. INTRODUCTION

IN RECENT years, considerable work has been conducted in multispectral imaging, in which more than three bands may be acquired, e.g., visible and infrared (IR). The reason for this increased interest is due to the fact that multispectral images can reveal much more information that are not available in a single band or color image. However, the acquisition of multispectral

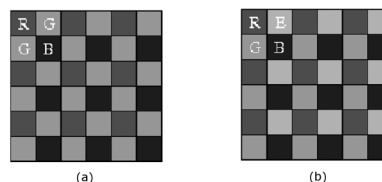


Fig. 1. Examples of CFAs: (a) Bayer array [1]; (b) Sony RGBE array [2].

images presents big challenges. To achieve an efficient solution for multispectral imaging, we study the potential of using multispectral filter arrays (MSFAs) in this paper.

The idea of using mosaic pattern to design a filter array instead of using a full multispectral camera is stimulated from the study findings of the human visual system as well as many other animal visual systems, in which different types of photoreceptors are organized into mosaics that tile the retina. The industry has been emulating this behavior by using the so-called color filter array (CFA) technique in the manufacture of digital color cameras. In this way, only one color component is measured at each pixel, and the missing spectral information can be estimated from neighboring pixels. Fig. 1 shows two examples of popularly used CFAs in the digital camera industry.

Similar to CFA, an MSFA is a mosaic pattern with each element being a wavelength-specific optical filter. By covering an MSFA over the sensing surface, a multispectral camera captures a scene such that each photodetector only captures one spectral band information. The resulting grayscale image is called the *mosaicked* image. To reconstruct the full multispectral image, a reconstruction operation, referred to as *MSFA demosaicking*, is required to estimate the missing spectral components at each pixel location. We call the resulted multispectral image the *reconstructed* image or the *demosaicked* image. Such a scheme can provide several advantages like low cost, exact registration, compact physical setup and strong robustness.

One of the earliest and most popularly used CFAs is the Bayer array [1] [shown in Fig. 1(a)]. Various demosaicking techniques have been derived [3]–[7] based on this array to obtain the full color image with minimum artifacts. However, the design philosophies of these algorithms are only applicable in the color domain, and cannot be directly generalized to MSFA demosaicking in the multispectral domain. Due to the increased number of spectral bands, the design of MSFAs as well as the restoration of multispectral data is more complicated. Therefore, the development of a generic algorithm with the capability of generalizing the mosaicking and demosaicking process of different multispectral images is of great importance.

Manuscript received July 12, 2005; revised March 8, 2006. This work was supported by the U.S. Army Space and Missile Defense Command under Grant DASG60-02-0001. This work was completed when R. Ramanath was with North Carolina State University. The associate editor coordinating the review of this manuscript and approving it for publication was Dr. Robert P. Loce.

L. Miao and H. Qi are with the Department of Electrical and Computer Engineering, Advanced Imaging and Collaborative Information Processing (AICIP) Group, The University of Tennessee, Knoxville, TN 37996 USA (e-mail: lmiao1@utk.edu; hqi@utk.edu).

R. Ramanath is with Texas Instruments, Inc., Plano, TX 75023 USA (e-mail: rajeev.ramanath@ieee.org).

W. E. Snyder is with the Department of Electrical and Computer Engineering, North Carolina State University, Raleigh, NC 27695 USA (e-mail: wes@eos.ncsu.edu).

Digital Object Identifier 10.1109/TIP.2006.877476

In this paper, we first give a short review of a binary tree-based generic MSFA generation method, which starts from a checkerboard pattern. By recursively separating the original checkerboard, the algorithm can generate desired MSFAs given the number of spectral bands and the probability of appearance (POA) of each band. We show that the two popular CFAs in Fig. 1 are simply special cases generated from the generic algorithm. Given the generated MSFA, we then design a generic demosaicking algorithm based on the same binary tree that generates the MSFA. The reconstructed images are evaluated from two perspectives: better reconstruction and better target discrimination.

In Sections II–V, we first analyze spectral correlations existed in multispectral images in Section II, then in Section III, we present the MSFA generation scheme, followed by the generic MSFA demosaicking algorithm in Section IV. Section V discusses the performance metrics and evaluates the experimental results. Conclusions are drawn in Section VI.

II. ANALYSIS OF SPECTRAL CORRELATIONS IN MULTISPECTRAL IMAGES

In this section, we conduct an in-depth analysis on the spectral correlations that might or might not exist in multispectral images, as this is one of the major hurdles in developing multispectral demosaicking algorithms. In the color domain, the correlation among the three color channels, i.e., red, green, and blue, play important roles in the demosaicking process, which has been elaborately investigated in a number of literature [6], [8]–[10]. In this section, we discuss two commonly used spectral correlations, namely *constant color difference (ratio)* and *constant edge location*, and analyze their applicability in the multispectral domain.

A. Constant Color Difference (Ratio)

One commonly used spectral correlation is the color ratio [11] or the color difference rule [8], which says that within a local image region, the ratios or differences between different color channels [i.e., red(blue)/green or red(blue)-green] are very similar. Instead of estimating the absolute value in the two chromatic color channels (i.e., red and blue), these algorithms estimate the color ratio or difference and then derive the chrominance value. Since the human visual system is more sensitive to color artifacts than to luminance or saturation errors, these schemes can reconstruct full color images with less visible artifacts and sharp edges. Although very promising in the color domain, these rules might not hold in the multispectral domain, which is to be validated in the following analysis.

We compare the ratio and difference correlations in a set of color and multispectral images. To keep it consistent, the term “color” is still used for defining ratio or difference between multispectral bands. We propose a metric *std* to quantify the interband correlation based on color difference as

$$std = \frac{\sum_{i=0}^{N_r-1} \sum_{j=0}^{N_c-1} \sqrt{\sum_{s,t \in \mathcal{N}_{i,j}} [d(i+s, j+t) - \bar{d}(i, j)]^2}}{N_r N_c}$$

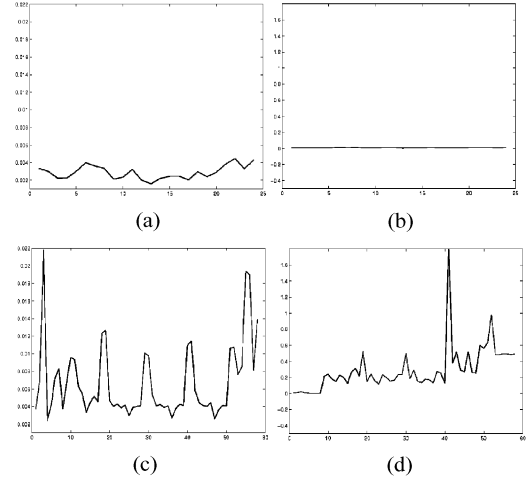


Fig. 2. Comparison of spectral correlation. The first two figures are color correlation and the last two figures show multispectral correlation. (a), (c) Difference based. (b), (d) Ratio based.

where N_r and N_c denote the number of image rows and columns, respectively, $\mathcal{N}_{i,j}$ is the neighborhood of pixel (i, j) , $d(i, j)$ represents the intensity difference between two spectral planes at the (i, j) location, and $\bar{d}(i, j)$ is the mean of the difference image within $\mathcal{N}_{i,j}$. The metric based on color ratio can be immediately obtained by substituting the color difference image d by the color ratio image. Note that the larger the *std*, the less similar the two spectral planes, and the less the correlation between spectral bands.

Twelve natural digital color images with rich high frequency information and two multispectral data sets described in Section V are used as testing images. For each color image, we obtain two difference (ratio) images, i.e., red-green (red/green) and blue-green (blue/green), and then calculate the *std* of each difference (ratio) image. In the multispectral domain, the difference (ratio) images are obtained from two adjacent spectral bands. The experimental results are demonstrated in Fig. 2, where the x axis is the index of color difference (ratio) images, and the y axis is the *std* value. Note that the multispectral images always possess much larger *std* than the color images. In other words, the spectral correlation based on color ratio or color difference in multispectral images is not so high as that in color images. Based on these observations, we predict that the existing CFA demosaicking techniques which explore color ratio or difference correlations cannot be simply extended to multispectral domain. This will be further validated in Section V.

B. Constant Edge Information

Another important interband correlation in the color domain is that all color bands possess similar edge information [5], [12]. Most wavelet-based demosaicking algorithms explore this correlation [13], [14]. In the multispectral domain, due to the wide wavelength range with each band capturing very different signatures, the edge information of different spectral bands would not be the same. Although it is true that different spectral bands might identify different edge locations, there should be no spurious edges. In other words, if the edges derived in all spectral



Fig. 3. Summation of edge images of seven spectral bands. Different colors represent different intensity values (1: red, 2: green, 3: blue, 4: cyan, 5: magenta, 6: yellow, 7: white).

bands are combined together, the resulting image would present all edge information of the scene.

One example is elaborated in Fig. 3, where we sum up seven edge images (they have intensity “1” at edge locations and “0” everywhere else) generated from a seven-band multispectral image using Canny edge detector, and different colors are used to denote different intensity values. Note for the worst case, if all the images possess different edge locations, then the summation image would have thick edges and all edge pixels have intensity one. However, we can see in Fig. 3 that only a few pixels possess intensity one and most edges still have single-pixel width, resulted from similar edge locations among different spectral bands. The exploration of this spectral correlation to improve reconstruction performance will be detailed in Section IV.

III. GENERIC MSFA GENERATION ALGORITHM

In the multispectral domain, the number of spectral bands and the wavelength range of each band usually vary depending on specific applications, compared to the fixed Red, Green, and Blue bands in the color domain. This has posed another challenge to the design of demosaicking algorithms in the multispectral domain. As mentioned before, although there has been considerable research in the field of demosaicking algorithm development, they are confined to the three-band Bayer CFA and cannot be directly extended to multispectral demosaicking. In order to develop a generic demosaicking algorithm that can cope with different application requirements, we need to study first the intrinsic properties of the MSFA and discover the underlying generic rules in generating MSFAs.

Given the number of spectral bands and the probability of appearance (POA) of each band, there are two important design criteria considered during the MSFA generation process, the *spectral consistency* and the *spatial uniformity*. To present the same reconstruction performance throughout the image plane, the *spectral consistency* requires that pixels should always have the same number of neighbors of a certain spectral band within a neighborhood of certain distance. The *spatial uniformity* requires that the filter array for each spectral band samples the entire image as evenly as possible. This requirement can avoid the degradation due to sparse sampling in a certain area. In order to meet both requirements, we have derived a generic algorithm for generating MSFA in [15]. Here, we briefly describe the algorithm, which consists of three components, binary tree generation, checkerboard separation, and leaf combination.

Fig. 4 illustrates the generation of a five-band MSFA using a binary tree with five leaves. Suppose we need to generate a K -band filter array and each spectral band has its specific

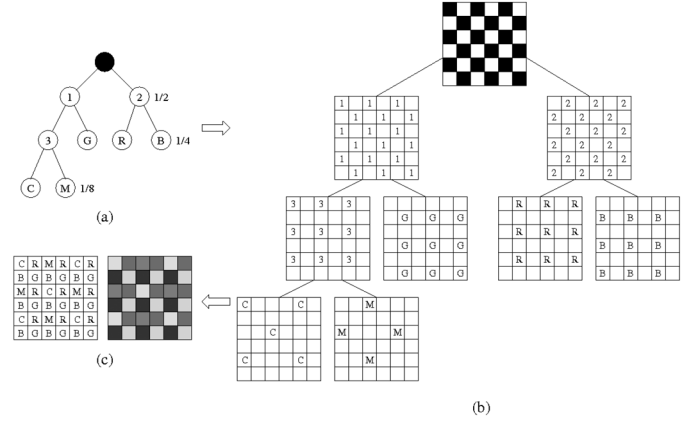


Fig. 4. Illustration of the generic MSFA generation process. (a) The binary tree. (b) Checkerboard separation. (c) Five-band MSFA generated by combining all the leaf patterns in (b).

POA r_1, r_2, \dots, r_K , where $r_i = (1/2^n)$, $n = 1, 2, \dots$, and $\sum_{i=1}^K r_i = 1$. First, we generate a binary tree such that it has K leaves and leaf i represents a spectral band with a POA of r_i . Fig. 4(a) shows a binary tree generated based on the specified probabilities $r = \{(1/4), (1/4), (1/4), (1/8), (1/8)\}$. The five leaf nodes correspond to the five spectral bands. For the sake of clarity, we use letters “R, G, B, C, M, Y, K...” to represent different spectral bands, which correspond to the leaf nodes in the binary tree. The internal nodes are denoted by numerical numbers, “1,” “2”... Based on this binary tree, we use a combination of decomposition and subsampling to generate a pattern satisfying the two requirements, as illustrated in Fig. 4(b). We treat the original checkerboard as the root, and each resulting pattern should correspond to one node in the binary tree (the same number or letter is used to indicate the corresponding relationship).

The decomposition is applied to the nodes at the even levels of the binary tree (including level zero, i.e., the root). The function of decomposition is to treat the pattern as a checkerboard and then divide the black and white blocks into two patterns, as illustrated in Fig. 4(b), where the label “1” and label “2” patterns are generated by decomposing the original checkerboard. The subsampling is to downsample the pattern by $2^{\frac{level+1}{2}}$ along the horizontal and vertical directions, where *level* refers to the level of the pattern being processed. For example, the label “3” and label “G” patterns are obtained by subsampling pattern “1,” and label “R” and label “B” patterns are the results of subsampling pattern “2” by 2.

Process the checkerboard until it has the same structure as the binary tree. The next step is to combine all the leaves to generate a mosaic pattern, as shown in Fig. 4(c), in which the left figure is obtained by combining all the leaf patterns in Fig. 4(b), and the right figure is the color representation. It can be shown that the two popularly used CFAs illustrated in Fig. 1 are actually special cases generated from the generic algorithm. For example, if we combine patterns “3,” “G,” “2” and assign different colors, the resulting mosaic pattern is the same as the Bayer array. The Sony RGBE array can be obtained by combining patterns “3,” “G,” “R,” and “B.” One unavoidable constraint associated with the binary tree-based method is that the

POA is limited to power of two. In the case that the probabilities do not fit the tree, we choose the closest approximation to substitute the original POAs. This approximation is necessary to satisfy the “uniform distribution” design requirement as in the rectangular domain, each pixel is either in a 4-neighborhood or an 8-neighborhood, that is, each pixel always has a number of neighbors equal to 2^n .

IV. GENERIC MSFA DEMOSAICKING ALGORITHM

Based on the MSFA generation algorithm described above, a generic demosaicking technique can be developed, which we refer to as the binary tree-based edge-sensing method (BTES). Using the same binary tree that generates the MSFA, this approach progressively estimates the missing pixel values, while utilizing the edge correlation information discussed in Section II-B. The generic demosaicking algorithm consists of three interrelated components:

- band selection—the determination of the interpolation order of different spectral bands;
- pixel selection—within each spectral band, the determination of the interpolation order of pixel locations;
- interpolation—the interpolation algorithm that uses the edge correlation information.

A. Band Selection

In the multispectral domain, since normally there are more than three spectral bands that need to be processed, the order of spectral band selection for interpolation needs to be predetermined. As illustrated in Section III, different spectral bands possess different POAs. It is intuitive that more detailed information is kept in the spectral band with higher POAs and that these bands contribute more in obtaining a reconstructed image that better resembles the real scene. In addition, the reconstructed image plane can be utilized to assist the interpolation of other spectral bands with lower POAs. Therefore, we start the interpolation by choosing a spectral band with the highest POA.

In the binary tree, band selection can be viewed as a process of selecting leaf nodes at different tree levels. We know the nodes at the same level possess the same POA and the deeper the level, the smaller the POA. To select spectral bands with their POAs in a descending order, we start from the first level of the binary tree. If there is a leaf node at this level, it will be the first selected spectral band for interpolation. This process continues as the tree level goes deeper. If there exist more than one leaf at a certain level, the selection order among these nodes is random. This band selection scheme facilitates our exploitation of spectral correlation (constant edge information). Since the band which preserves the edge information the best will be interpolated first, the estimation of other bands can utilize the edge information of the first interpolated image plane provided that different bands possess similar edge locations.

B. Pixel Selection

In most demosaicking schemes in the color domain, the missing pixels are estimated only based on known pixel values. However, in the multispectral domain, more missing pixels are present in each spectral band and only using known MSFA samples will not generate good results. In this paper, we present a

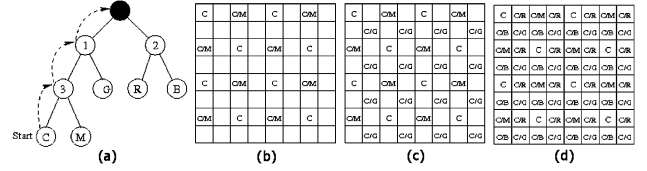


Fig. 5. Illustration of pixel selection process of band “C.” (a) The directed dash lines indicate the trace of traversal. (b) The “C” values at pixel locations with known “M” are first estimated based on known “C”s. (c) The “C” values at pixel locations with known “G” are second estimated based on both known and estimated “C”s from (b). (d) At node “1,” pixel locations at “2” positions are selected, which are combinations of pixel locations at node “R” and “B.”

“progressive” demosaicking method, taken into consideration of the sparse samples exist in MSFA patterns. That is, part of the missing pixel values are estimated first, then the estimated pixel values together with the known MSFA samples are used to estimate other unknown pixel values. In this way, it is very important to determine which pixel locations are estimated first and which are the next.

To effectively utilize the structural features of different patterns presented in the binary tree, we develop a pixel selection scheme, which is a binary tree traversal process. Starting from one of the leaf patterns selected in the band selection component, the algorithm first interpolates the missing band information at pixel locations where its sibling pattern locates, then the algorithm goes up one level of the binary tree and finds the sibling of its parent pattern. If its parent’s sibling is an internal node, then the leaf patterns of the subtree under this sibling pattern are investigated. This process continues until the root node is visited. It can be seen that, at each step, after interpolating the selected pixel locations, the resulted pattern is the same as the parent pattern. Thus, the pixel selection scheme guarantees that all the intermediate patterns during the demosaicking process are those presented in the binary tree.

Fig. 5 illustrates an example of the pixel selection process, in which we aim to reconstruct spectral band “C.” Starting from node “C,” we first select the pixel locations where its sibling pattern “M” locates [Fig. 5(b)]. We use “C/M” to denote the interpolation of the “C” value at the “M” location. Then we go up one level to node “3” and select pixel locations where its sibling pattern “G” located [Fig. 5(c)]. Continuing this process one more level will lead us to the internal node “2,” which is the combination of pixel locations in pattern “R” and “B” [Fig. 5(d)]. The directed dash lines in Fig. 5(a) indicate the trace of traversal and the resulting pattern at each step is shown in Fig. 5(b)–(d), respectively. Note that the intermediate patterns are determined by the traversal trace on the binary tree, and the POA at each step is given by $\{1/2^{level}, 1/2^{level-1}, \dots, 1/2, level > 1\}$.

C. Interpolation

Given certain pixel location within certain spectral band, selected based on the band and pixel selection scheme described above, the last issue to be considered is how to estimate the missing pixel values based on neighboring pixel information. The key to the design of a generic demosaicking algorithm is the application of the binary tree. We need to identify a basic pattern first and develop the demosaicking algorithm based on this

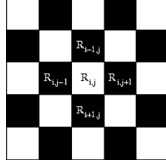


Fig. 6. Basic pattern.

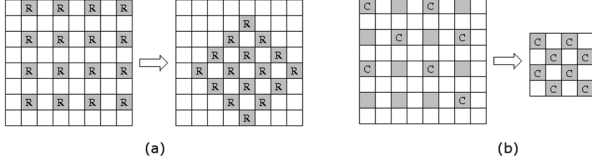


Fig. 7. Illustration of forward transform. (a) Transform of pattern "R" by rotating 45° clockwise with the upper-left corner being the origin. (b) Transform of pattern "C" through downsampling by 2.

pattern. In addition, we need to find a transformation that transforms all patterns present in the binary tree to the basic pattern. The operation of transforming a certain pattern to the basic pattern is called the *forward transform* and the reverse process the *inverse transform*. For a pattern in the binary tree, if we apply forward transform first, followed by interpolating the missing pixel values and the inverse transform, the resulting pattern is exactly the same as its parent. We name this three-step processes (i.e., forward transform, interpolation, and inverse transform) the *one-step interpolation*. The reconstruction of a certain spectral band at level *level* of the binary tree consists of *level* one-step interpolations. Therefore, we only need to derive an algorithm to interpolate the basic pattern.

The basic pattern we identified is illustrated in Fig. 6 and all patterns in the binary tree can be transformed into this basic pattern through two operations, namely, resampling and resampling combined with rotation. The basic pattern is actually the decomposed result of the original checkerboard, where the spectral information at the black pixels are known, and the intensity value at spatial location (i, j) is denoted by $R_{i,j}$.

For patterns at the odd levels of the binary tree, only resampling is needed to transform them to the basic pattern, that is, the pattern need to be downsampled by $2^{(level-1)/2}$, $level > 0$. To transform patterns at the even levels of the binary tree, the pattern should be first downsampled by $2^{level/2-1}$, $level > 1$ and then rotated clockwise or counterclockwise by 45°. For instance, the pattern "R" can be transformed to the basic pattern by simply rotating 45°, and the pattern "C" also turns into a basic pattern after downsampled by 2, i.e., only keep the odd number columns and rows. These operations are illustrated in Fig. 7(a) and (b), respectively.

One of the most challenging issue in demosaicking is the preservation of edge information. This issue becomes more difficult to solve in the multispectral domain as each spectral band in general has a lower spatial resolution. In this paper, we adopt the idea of using weighted sum of neighboring pixels, which has been successfully used in CFA demosaicking [8], [11]. In the basic pattern, suppose we want to estimate the pixel value at the center denoted by $R_{i,j}$. We need information from its neighboring pixels, and the contributions from the four nearest

neighbors, i.e., " $R_{i-1,j}$," " $R_{i,j+1}$," " $R_{i+1,j}$," and " $R_{i,j-1}$," would be more important than others. The weights of these four pixels are estimated based on their edge magnitudes, and the larger the edge magnitude, the less the contribution from the corresponding neighbor. The weights of two neighboring pixels along the vertical direction are calculated by

$$V : W_{m,n} = \left(1 + |R_{m+2,n} - R_{m,n}| + |R_{m-2,n} - R_{m,n}| + \frac{1}{2}|R_{m-1,n-1} - R_{m+1,n-1}| + \frac{1}{2}|R_{m-1,n+1} - R_{m+1,n+1}| \right)^{-1}$$

where $m \in \{i-1, i+1\}$, $n = j$, and that along the horizontal direction is

$$H : W_{m,n} = \left(1 + |R_{m,n+2} - R_{m,n}| + |R_{m,n-2} - R_{m,n}| + \frac{1}{2}|R_{m+1,n-1} - R_{m+1,n+1}| + \frac{1}{2}|R_{m-1,n-1} - R_{m-1,n+1}| \right)^{-1}$$

with $m = i$, $n \in \{j-1, j+1\}$. The estimation of center pixel is given by the weighted sum of the four nearest neighbors

$$\hat{R}_{i,j} = \frac{\sum_{s,t(|s+t|=1)} W_{i+s,j+t} R_{i+s,j+t}}{\sum_{s,t(|s+t|=1)} W_{i+s,j+t}}$$

where $\hat{R}_{i,j}$ represents the estimated value at (i, j) position.

This edge-sensing approach interpolates the unknown according to pixel weights derived from edge information. Thus, the estimation of edge information directly affects the quality of reconstructed images. In multispectral imaging, as the number of spectral bands increases, the spatial resolution decreases in certain spectral bands and the edge information based on the low resolution spectral band information would not be reliable. As analyzed before, the edge information in different spectral bands are either similar or partly overlapped. The spectral band with the highest POA preserves the edge information the best. Therefore, the edge information in high resolution spectral band can be used to calculate the weights in low resolution spectral band since the band selection scheme guarantees the high resolution spectral bands are reconstructed first.

V. PERFORMANCE EVALUATION

A. Performance Metrics

The performance of a certain MSFA demosaicking algorithm can be evaluated from two perspectives: the reconstruction accuracy and the target classification accuracy.

There have been several commonly used metrics in literature to measure the reconstruction accuracy, including root mean-square error (RMSE), peak signal-to-noise ratio (PSNR), and

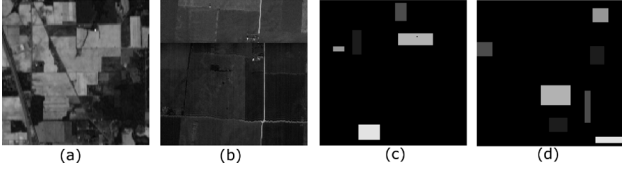


Fig. 8. Visualization of the two real multispectral data sets and the corresponding class labels: (a) 92AV3C9 (band 1); (b) FLC1 (band 3); (c) class label of 92AV3C9, red-grass, green-tower, blue-corn, cyan-soil, yellow-hay; (d) class label of FLC1, red-oats, green-corn, blue-red clover, cyan-bare soil, yellow-wheat.

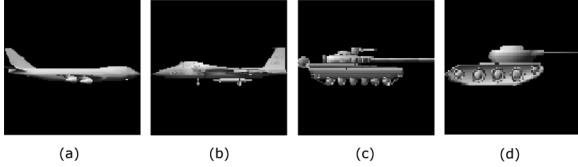


Fig. 9. Four examples of the eight synthetic multispectral images.

subjective comparison, etc. To measure the fidelity of the demosaicked images, we use the RMSE metric defined as

$$\text{RMSE} = \sqrt{\frac{1}{N_b N_r N_c} \sum_{k=1}^{N_b} \sum_{i=0}^{N_r-1} \sum_{j=0}^{N_c-1} [\hat{f}_k(i, j) - f_k(i, j)]^2}$$

where \hat{f}_k represents the k th spectral plane of the demosaicked image and f_k that of the original one; N_b , N_r , and N_c denote the number of spectral bands, rows, and columns of the multispectral image respectively.

In order to evaluate the reconstructed images regarding to the target detection or recognition rate, classification is carried out on both the original and the demosaicked images. The experimental results show that these two metrics reveal different performance aspects.

B. Description of Multispectral Test Data Sets

Two sets of real multispectral data [16], popularly used in multispectral image analysis, are used to evaluate the proposed method. Fig. 8(a) and (b) displays one spectral band of each data set [Fig. 8(b) is only a small segment of the original data sets]. The 92AV3C9 contains nine spectral bands selected from a June 1992 AVIRIS data set [17]. The Flightline C1 (FLC1) image was collected with an airborne scanner in June 1966, which contains 12 spectral bands with the wavelength varying from 0.4 to 1.0 μm . These two data sets contain a significant number of vegetative species or ground cover classes and have “ground truth” available.

In addition, the eight synthetic data sets are generated by selecting from hyperspectral images using the band selection method discussed in [18]. The original hyperspectral images are generated by a simulator developed at North Carolina State University [19]. Each multispectral image contains 7 bands and has a different object. Fig. 9 shows four examples of the eight targets.

To study the MSFA mosaicking and demosaicking performance generalized to different numbers of spectral bands, we

form new multispectral images by selecting different numbers of bands from each of the above multispectral data sets. For example, we create five multispectral images from the 92AV3C9 data, and they contain three, four, five, six, and seven bands, respectively. The band selection is performed using the multispectral system [16] developed at the Purdue University. The created multispectral images are first sampled using the derived MSFAs to generate the mosaicked images. Without loss of generality, we keep the POA of each band as equal as possible, which can be implemented by a balanced binary tree. Then we apply different demosaicking algorithms to reconstruct the full multispectral data.

C. Selection of the Training and the Testing Data

For the two real multispectral data sets, we select five ground cover classes for each of the data sets, according to the ground truth provided in [20] and [17]. Fig. 8(c) and (d) shows their corresponding class labels, where the five different colors correspond to the five different classes. For each cover class, we use half of the pixels to train the classifier and the other half serves as the testing samples.

As to the synthetic data set, we treat each target as one class, which gives us in total eight classes. The training data set also consists of half of the target pixels uniformly selected from each target, and the rest of the target pixels are used as the testing data.

To perform classification, a simple k -nearest neighbor (kNN) classifier [21] is used, in which k denotes the number of neighbors and is normally calculated by $k = \sqrt{n}$ (n is the number of training samples). kNN assigns the unknown sample to the same class as the class of the nearest neighbor(s) in the training set. The spectral response at each pixel location is used as the feature vector to classify the corresponding pixel. This is based on the assumption that different materials should have different spectral signatures.

D. Experimental Results

We design two sets of experiments to evaluate the performance of the BTES method. In the first experiment, we investigate the effectiveness of incorporating the binary tree and the edge information in the demosaicking process. In the second experiment, we compare the proposed BTES method with three advanced CFA demosaicking approaches published recently.

1) *The Effectiveness of Binary Tree and Edge Sensing Method:* The proposed BTES approach integrates the binary tree-based scheme and the edge-sensing interpolation. In order to investigate the effectiveness of these two features, we implement three demosaicking methods that are variants of BTES, including the classical bilinear interpolation (BI) without using either features, the binary tree-based bilinear interpolation (BTBI), and the edge-sensing interpolation without the binary tree consideration (ES). Edge-sensing-based demosaicking methods (i.e., ES and BTES) take into account the different weights of each individual neighbors when estimating the missing information, while nonedge-sensing methods simply treat the neighboring pixels equally. Binary tree-based methods (i.e., BTBI and BTES) estimate the missing pixels based on not only *known* MSFA samples, they also use *estimated* MSFA samples obtained following the binary tree structure. The

TABLE I
CLASSIFICATION ACCURACY (%) OF REAL MULTISPECTRAL DATA OF DIFFERENT METHODS

Images	92AV3C9						FLC1					
	3-band	4-band	5-band	6-band	7-band	Avg.	3-band	4-band	5-band	6-band	7-band	Avg.
ORG	90.30	91.80	90.80	91.63	89.63	90.83	76.74	80.79	82.55	83.19	83.00	81.25
BTES	88.96	93.65	91.14	91.30	90.47	91.10	78.43	82.56	84.39	85.93	85.44	83.35
ES	88.12	92.30	90.63	89.80	88.46	89.86	77.83	82.14	83.88	85.29	84.67	82.76
BTBI	86.79	92.81	89.63	90.80	88.63	89.73	77.79	82.32	83.75	85.24	84.56	82.73
BI	86.78	92.14	90.30	90.97	88.79	89.79	77.47	81.84	83.53	84.88	84.17	82.38

TABLE II
RMSE OF DEMOSAICKED REAL MULTISPECTRAL DATA OF DIFFERENT METHODS

Images	92AV3C9						FLC1					
	3-band	4-band	5-band	6-band	7-band	Avg.	3-band	4-band	5-band	6-band	7-band	Avg.
BTES	8.92	18.88	18.06	16.96	19.28	16.41	3.50	4.27	4.48	4.65	4.77	4.33
ES	9.20	18.85	17.87	17.47	19.73	16.62	3.85	4.48	4.90	5.24	5.45	4.78
BTBI	9.11	18.82	18.32	17.30	19.61	16.63	4.02	4.60	4.80	5.05	5.21	4.74
BI	9.30	18.90	18.39	17.41	19.75	16.75	3.99	4.66	4.95	5.27	5.47	4.87

TABLE III
CLASSIFICATION ACCURACY (%) OF SYNTHETIC DATA

Image	3-band	4-band	5-band	6-band	7-band	Avg.
ORG	67.71	69.14	69.92	70.83	73.14	70.15
BTES	61.98	66.82	68.79	69.24	70.79	67.52
ES	62.04	66.02	66.79	66.48	67.54	65.77
BTBI	60.03	65.84	65.90	64.37	65.79	64.39
BI	60.54	65.15	65.50	64.80	65.71	64.34

TABLE IV
RMSE OF DEMOSAICKED SYNTHETIC DATA

Image	3-band	4-band	5-band	6-band	7-band	Avg.
BTES	4.10	3.78	4.36	5.40	6.63	4.85
ES	4.37	4.05	4.89	6.28	7.80	5.48
BTBI	4.39	4.03	4.77	6.16	7.70	5.41
BI	4.43	4.07	4.87	6.30	7.88	5.51

purpose of this experiment is to evaluate the effectiveness of these two features using the RMSE metric and the classification accuracy metric.

The classification accuracy generated by BTES and its three variants on the real multispectral data is summarized in Table I, and the results of the synthetic data are listed in Table III. Tables II and IV show the RMSE of different demosaicking methods on both data sets. From these four tables, we make the following three observations. First of all, among the demosaicking algorithms evaluated, BTES, in most cases and on average, outperforms its three variants from both classification accuracy and RMSE perspectives. We also observe that the binary tree-based methods (i.e., BTES and BTBI) outperform the corresponding schemes without binary tree considerations (i.e., ES and BI).

Another important observation is that the classification performance cannot be improved by simply increasing the number of spectral bands. As illustrated in Table I, the four-band image gives the highest accuracy for the 92AV3C9 data, while the six-band image is the best for the FLC1 data. There are two underlying reasons for this phenomenon. First, the newly introduced spectral information does not guarantee to increase the class separability of multispectral data. Second, there is a

TABLE V
CLASSIFICATION IMPROVEMENT BETWEEN DEMOSAICKED AND ORIGINAL SYNTHETIC IMAGES OF NOISY (ipr_n) AND NOISE-FREE (ipr) CASES

Image	3-band	4-band	5-band	6-band	7-band
acc_{or}	67.71	69.14	69.92	70.83	73.14
acc_{de}	61.98	66.82	68.79	69.24	70.79
ipr	-8.46	-3.37	-1.62	-2.26	-3.21
acc_{or_n}	39.67	51.54	56.44	57.00	57.77
acc_{den}	62.18	66.75	67.87	66.58	68.36
ipr_n	56.75	29.5	20.25	16.82	18.34

tradeoff between the spectral and the spatial resolution when using the MSFA technique. The extra spectral information is introduced at the cost of reducing the reconstruction performance due to lower spatial resolution. This observation can be further verified by investigating the RMSE of the reconstructed images from Tables II and IV. It can be seen that the RMSE values increase as the number of spectral bands increases, that is, the lower the spatial resolution, the worse the reconstruction performance.

Our third observation is that the classification accuracy of the demosaicked images is comparable to that of the original data. Interestingly, for the real multispectral scene, in most cases, the reconstructed images present higher classification accuracy. However, this is not true for the synthetic data, in which case the original images always generate the highest classification performance. This phenomenon is related to both the characteristics of the selected data sets as well as the intrinsic feature of the mosaicking and the demosaicking process. We realize that the real multispectral images are acquired in real world environment interfered by both the sensor noise and all kinds of other environmental effects, compared to the synthetic data generated with a perfect zero interference. We further notice that the mosaicking and the demosaicking process combined together act as a smoothing filter (interpolation of missing pixel information from weighted summation of neighbors), which actually suppresses both noise and outliers in the original images. Therefore, the demosaicked real multispectral images, with less noise and outliers compared with the original data, would be able to

TABLE VI
RMSE COMPARISON BETWEEN BTES AND THREE CFA DEMOSAICKING ALGORITHMS

Image	747	dc10	f15	mig	tank0	tank1	tank2	tank3	Avg.
BTES	3.46	3.77	4.40	4.08	6.21	4.11	4.71	3.71	4.31
Algo.[6]	7.66	7.37	8.28	8.89	9.64	7.17	8.62	7.33	8.11
Algo. [8]	3.01	3.09	3.88	4.79	5.72	2.49	4.61	2.36	3.74
Algo. [10]	4.67	4.58	5.26	5.71	6.65	4.82	5.60	4.55	5.23

generate higher classification accuracy. On the other hand, due to the loss of high frequency information, the demosaicked synthetic data would yield lower classification performance than the original ones, which contains all the information of the demosaicked images.

To validate the above analysis, we add 20-dB Gaussian noise to the synthetic images and then perform the mosaicking and demosaicking process. The classification accuracy improvement, defined as $\text{ipr} = (\text{acc}_{\text{de}} - \text{acc}_{\text{or}}) / \text{acc}_{\text{or}} \times 100\%$, where acc_{de} and acc_{or} denote the classification accuracy using the demosaicked image and the original image, respectively, with and without noise cases are summarized in Table V, in which acc_{den} and acc_{orn} denote the classification accuracy of the noisy data. We relist the classification results of pure signals without noise in Table V to facilitate comparison. Note that, for the images without noise, the classification improvements are all negative; that is, the demosaicked images produce lower classification accuracy than the original data. However, for the noisy data, there exists up to 56.75% improvement on the classification performance of the demosaicked images over the original noisy data. These results verify our previous analysis on why the original data do worse than the demosaicked images. In real-world applications, it is impossible to generate a perfect, noise free image. Most likely, the captured images would contain different types of noises, for which the demosaicked images after the process of mosaicking and demosaicking can provide comparable classification performance as the original data.

2) *Comparison With Advanced CFA Demosaicking Algorithms*: The purpose of this experiment is to evaluate the proposed BTES algorithm with existing rich collection of CFA demosaicking algorithms. We selected three advanced CFA demosaicking approaches [6], [8], [10] recently published in the literature. These techniques effectively utilize the spectral and spatial correlations to suppress artifacts. Algorithm [8] uses edge-directed interpolation and effectively exploits the color difference correlation, in which the green channel is interpolated first, and the red and blue channels are interpolated with the green band information as a correction term. The postprocessing step uses the color difference information (i.e., green-red and green-blue) to reduce color artifacts. Algorithm [10] formulates the demosaicking problem as an iterative process of reconstructing correlated signals (i.e., the green plane and the red/blue plane) from their subsampled versions. Another reconstruction approach [6] introduces wavelet analysis to decompose the original image into detail subbands. The algorithm enforces similar high-frequency information for the three color planes by updating the detail subband of the red and blue channels so that they are within a threshold to that of the green channel.

TABLE VII
CLASSIFICATION ACCURACY (%) OF ORIGINAL AND RECONSTRUCTED IMAGE USING DIFFERENT DEMOSAICKING ALGORITHMS

Algo.	Original	BTES	Algo.[6]	Algo.[8]	Algo.[10]
<i>acc</i>	67.71	61.98	53.77	57.72	50.31

In order to perform a fair comparison, instead of modifying the algorithms to deal with multiple bands, we choose three adjacent bands (one visual band and two infrared bands) from multispectral images and then treat them as the three color planes. We observe that the visual band contains more detail information; therefore, we use the visual band as the green channel and the other two infrared bands as the red and blue channels.

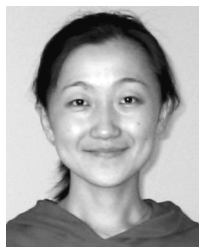
The quantitative comparisons based on the RMSE and the classification accuracy are summarized in Tables VI and VII, respectively. From the RMSE comparison, we see that algorithm [8], in general, generates the best results, while the BTES algorithm ranks the second and outperforms algorithm [10] and [6] by producing lower RMSE. However, by investigating the classification results, we note that the BTES approach performs the best, and gives higher classification accuracy than other CFA demosaicking methods. Algorithm [8] provides better classification performance than [6] and [10], whose classification accuracy are much lower than that of the original data. In summary, the BTES generic approach provides the highest classification accuracy although with a slightly worse RMSE performance compared to algorithm [8]. However, the BTES algorithm is a generalized approach, while the CFA demosaicking methods are confined to the color domain and cannot be directly extended to MSFA demosaicking.

VI. CONCLUSION

In this paper, we studied the potential of using MSFA techniques in multispectral imaging by developing generic mosaicking and demosaicking algorithms. The binary tree-driven MSFA generation process guarantees that the pixel distributions of different spectral bands are uniform and highly correlated. These spatial features facilitate the design of the generic demosaicking algorithm based on the same tree, which considers three interrelated issues: band selection, pixel selection, and interpolation. The development of a generic algorithm enables the cost-effective multispectral imaging. We evaluate the reconstructed images from two perspectives: better reconstruction and better target detection. The experimental results demonstrate that the mosaicking and demosaicking processes preserve the classification accuracy effectively for real world data. This result further supports that the MSFA technique is a feasible solution for multispectral cameras.

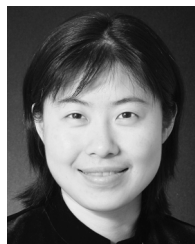
REFERENCES

- [1] E. B. Bayer, "Color Imaging Array," U.S. Patent 3 971 065, 1976.
- [2] Sony Press. [Online]. Available: <http://www.sony.net/SonyInfo/News/Press/200307/03-029E/>
- [3] R. Ramanath, W. E. Snyder, and G. L. Bilbro, "Demosaicking methods for Bayer color arrays," *J. Electron. Imag.*, vol. 11, no. 3, pp. 306–315, Jul. 2002.
- [4] R. Lukac, K. Martin, and K. N. Plataniotis, "Demosaicked image post-processing using local color ratios," *IEEE Trans. Circuits Syst. Video Technol.*, vol. 14, no. 6, pp. 914–920, Jun. 2004.
- [5] L. Chang and Y. P. Tan, "Effective use of spatial and spectral correlations for color filter array demosaicking," *IEEE Trans. Consum. Electron.*, vol. 50, no. 1, pp. 355–365, Feb. 2004.
- [6] B. K. Gunturk, Y. Altunbasak, and R. M. Mersereau, "Color plane interpolation using alternating projections," *IEEE Trans. Image Process.*, vol. 11, no. 9, pp. 997–1013, Sep. 2002.
- [7] X. Li and M. T. Orchard, "New edge-directed interpolation," *IEEE Trans. Image Process.*, vol. 10, no. 10, pp. 1521–1527, Oct. 2001.
- [8] W. Lu and Y. P. Tan, "Color filter array demosaicking: New method and performance measures," *IEEE Trans. Image Process.*, vol. 12, no. 10, pp. 1194–1210, Oct. 2003.
- [9] X. Wu and N. Zhang, "Primary-consistent soft-decision color demosaicking for digital cameras," *IEEE Trans. Image Process.*, vol. 13, no. 9, pp. 1263–1274, Sep. 2004.
- [10] X. Li, "Demosaicking by successive approximation," *IEEE Trans. Image Process.*, vol. 14, no. 3, pp. 370–379, Mar. 2005.
- [11] R. Kimmel, "Demosaicking: Image reconstruction from color ccd samples," *IEEE Trans. Image Process.*, vol. 8, no. 9, pp. 1221–1228, Sep. 1999.
- [12] X. Wu, W. K. Choi, and P. Bao, "Color restoration from digital camera data by pattern matching," *Proc. SPIE*, vol. 3018, pp. 12–17, 1997.
- [13] J. Driesen and P. Scheunders, "Wavelet-based color filter array demosaicking," in *Proc. IEEE Int. Conf. Image Processing*, Oct. 2004, vol. 5, pp. 3311–3314.
- [14] L. Chen, K. H. Yap, and Y. He, "Color filter array demosaicking using wavelet-based subband synthesis," in *Proc. IEEE Int. Conf. Image Processing*, Sep. 2005, vol. 2, pp. 1002–1005.
- [15] L. Miao and H. Qi, "The design and evaluation of a generic method for generating mosaicked multispectral filter arrays," *IEEE Trans. Image Process.*, vol. 15, no. 9, pp. 2780–2791, Sep. 2006.
- [16] Laboratory for Applications of Remote Sensing. [Online]. Available: <http://www.lars.purdue.edu>
- [17] D. Landgrebe, "Multispectral Data Analysis: A Signal Theory Perspective," 1998. [Online]. Available: <http://dynamo.ccn.purdue.edu/~biehl/MultiSpec/Signal-Theory.pdf>
- [18] R. Ramanath, W. E. Snyder, and H. Qi, "Mosaic multispectral focal plane array cameras," presented at the SPIE Defense and Security Symp. Orlando, FL, Apr. 12–16, 2004.
- [19] R. Ramanath, "A Framework for Object-characterization and Matching in Multi- and Hyperspectral Imaging Systems," Ph.D. dissertation, Dept. Elect. Comput. Eng., North Carolina State Univ., Raleigh.
- [20] D. Landgrebe, "Multispectral Data Analysis: A Moderate Dimension Example," 1997. [Online]. Available: <http://dynamo.ccn.purdue.edu/~biehl/MultiSpec/Moderate-Dimension.pdf>
- [21] R. Duda, P. Hart, and D. Stork, *Pattern Classification*. New York: Wiley, 2000.



Lidan Miao (S'04) received the B.S. and M.S. degrees in electrical engineering from Sichuan University, China, in 2000 and 2003, respectively. She is currently pursuing the Ph.D. degree in the Department of Electrical and Computer Engineering, University of Tennessee, Knoxville.

Her current research interests include signal and image processing, pattern recognition, and remote sensing.



Hairong Qi (SM'05) received the B.S. and M.S. degrees in computer science from Northern JiaoTong University, Beijing, China, in 1992 and 1995, respectively, and the Ph.D. degree in computer engineering from North Carolina State University, Raleigh, in 1999.

She is currently an Associate Professor with the Department of Electrical and Computer Engineering, University of Tennessee, Knoxville. She has published over 70 technical papers in archival journals and refereed conference proceedings, including a coauthored book on machine vision. Her current research interests are advanced imaging and collaborative processing in sensor networks, hyperspectral image analysis, and bioinformatics.

Dr. Qi is a member of Sigma Xi and SPIE. She is the recipient of the National Science Foundation CAREER award and the Chancellor's Award for Professional Promise in Research and Creative Achievement. She serves on the editorial board of *Sensor Letters* and is the Associate Editor for *Computers in Biology and Medicine*. She coedited a special issue of the *Journal of The Franklin Institute* on distributed sensor networks for real-time systems with adaptive configuration.



Rajeev Ramanath (M'03) received the B.Eng. degree in electrical and electronics engineering from the Birla Institute of Technology and Science, Pilani, India, in 1998, the M.S. degree in electrical engineering from North Carolina State University (NCSU), Raleigh, in 2000 for his work titled "Interpolation Methods for Bayer Color Arrays," and the Ph.D. degree in electrical engineering from NCSU in 2003 for his dissertation titled "A Framework for Object-characterization and Matching in Multi- and Hyperspectral Imaging Systems."

After a one-year-long postdoctoral position with the Electrical and Computer Engineering Department, NCSU—during which he taught two classes: an advanced graduate-level course on statistical pattern recognition and an introductory junior-level course on linear systems—he joined Texas Instruments, Inc., Plano, TX, working in the DLP(r) Products Algorithm Development Group. His research interests include computer vision, image and signal processing, demosaicking in digital color cameras, color science, and automatic target recognition.



Wesley E. Snyder (SM'80) received the B.S. degree in electrical engineering from North Carolina State University, Raleigh, in 1968, and the M.S. and Ph.D. degrees in electrical engineering from the University of Illinois at Urbana-Champaign, Urbana, in 1971 and 1975, respectively.

His research interests include image processing and analysis. His best-known work concerns pattern recognition with applications to robot vision, and recent efforts involve implementing computer vision algorithms in neural networks and medical image processing. He has written over 100 scientific papers and is the author of the book *Industrial Robots* (Englewood Cliffs, NJ: Prentice-Hall, 1985).

Dr. Snyder was a founder of both the IEEE Robotics and Automation Society and the IEEE Neural Networks Council. He has served as an advisor to the National Science Foundation, NASA, Sandia Laboratories, and the U.S. Army Research Office.